

# Exact Markovian Dynamics in Quantum Circuits

He-Ran Wang,<sup>1</sup> Xiao-Yang Yang,<sup>1,2</sup> and Zhong Wang<sup>1</sup>

<sup>1</sup>*Institute for Advanced Study, Tsinghua University, Beijing 100084, People's Republic of China*

<sup>2</sup>*Department of Physics, Tsinghua University, Beijing 100084, People's Republic of China*

Characterizing non-equilibrium dynamics in quantum many-body systems is a challenging frontier of physics. In this work, we systematically construct solvable non-integrable quantum circuits that exhibit exact Markovian subsystem dynamics. This feature thus enables accurately calculating local observables for arbitrary evolution time. Utilizing the influence matrix method, we show that the effect of the time-evolved global system on a finite subsystem can be analytically described by sequential, time-local quantum channels acting on the subsystem boundary. The realization of exact Markovian property is facilitated by a solvable condition on the underlying two-site gates in the quantum circuit. We further present several concrete examples with varying local Hilbert space dimensions to demonstrate our approach.

In isolated quantum many-body systems driven out of equilibrium, thermalization typically occurs, where local observables relax to their thermal-averaged expectation values after a finite time. Heuristically, the global system serves as a thermal bath for the local subsystem [1–5]. On the other hand, various counterexamples of thermalization have been extensively studied, including integrable models [6], many-body localization [7, 8], and quantum many-body scars [9–11]. However, for both scenarios (following or violating thermalization), it poses a formidable challenge to accurately quantify the influence of the time-evolved macroscopic many-body system on its own subsystem, due to the exponentially large Hilbert space dimension in the thermodynamic limit (TL) and the quantum memory effects brought by the non-Markovianity.

Recently, progress has been made in quantum circuits, where the unitary evolution is discretized to sequences of local unitary gates. In particular, Refs. [12–17] have developed an efficient tensor-network approach to trace out the system, and encode the influence on the subsystem into the fixed point of the spatial transfer matrix, which is also known as the *influence matrix* [16, 17]. However, the intrinsic complexity of many-body dynamics typically leads to complicated influence matrices as the evolution time grows, restricting rigorous numerical and analytical treatment within this approach [18].

In this paper, we introduce a novel approach to systematically constructing 1+1 D non-integrable quantum circuits exhibiting exact Markovian subsystem dynamics. We introduce a solvable condition for the underlying unitary gates allowing for efficient contractions of quantum-circuit tensor networks for arbitrary evolution time. We show that the time-evolved system can be traced out to a closed-form influence matrix in the Matrix Product State (MPS) representation, thus enabling numerical calculations of subsystem dynamics in an exact fashion. Remarkably, we interpret the influence matrix as time-local quantum channels acting on the subsystem boundary, implying the role of the system as a *Markovian bath*. Hence, our work discovers new principles leading to subsystem Markovian property, and provides a promising test-ground to explore rich phenomena in quantum many-body dynamics through analytical tools.

*The setup.*— In this paper, we consider quantum circuits on a 1D lattice, where each site is labeled by an integer  $x$ . We as-

sociate a  $q$ -dimensional Hilbert space  $\mathcal{H}_q$  for each site, with a basis:  $\{|a\rangle, a = 0, 1, \dots, q-1\}$ . The system is prepared in an initial state  $|\Psi_{\text{in}}\rangle$  and undergoes discrete time evolution. For each time step, the global unitary operator is  $\mathbb{U} = \mathbb{U}_{\text{odd}}\mathbb{U}_{\text{even}}$ , where  $\mathbb{U}_{\text{odd(even)}} = \bigotimes_{x \in \text{odd(even)}} U_{x,x+1}$ .  $U_{x,x+1}$  are two-site gates acting locally on  $x$  and  $x+1$ . As indicated by the form of  $\mathbb{U}$ , the local gates are arranged in a brickwork architecture.

For the sake of convenience in depiction, we fold the forward and backward branches of time evolution [see Fig. 1(a)]. By folding, each tensor is superimposed on its complex conjugate. The folded two-site unitary gate acting on the doubled space is defined as the following four-leg tensor:

$$\begin{array}{c} c, c' \\ \diagup \quad \diagdown \\ \text{---} \square \text{---} \\ \diagdown \quad \diagup \\ a, a' \end{array} \begin{array}{c} d, d' \\ \diagup \quad \diagdown \\ \text{---} \square \text{---} \\ \diagdown \quad \diagup \\ b, b' \end{array} = U_{ab}^{cd} \left( U_{a'b'}^{c'd'} \right)^*, \quad (1)$$

where  $a, b, c, d$  ( $a', b', c', d'$ ) denote the basis states in the forward (backward) branch.

We focus on a certain class of initial states on the composite system L-R, where L (R) for the left (right), as shown in Fig. 1(b). For later convenience, we set the location of the leftmost site on R as the origin point  $x = 0$ . The global unitary operator admits a decomposition as  $\mathbb{U} = \mathbb{U}_{\bar{R}}\mathbb{U}_R$ , where  $\mathbb{U}_R$  acts solely on R, and  $\mathbb{U}_{\bar{R}}$  acts on L and the boundary across the two regions. Meanwhile, we assume that the overall initial state can be decomposed as  $|\Psi_{\text{in}}\rangle = \sum_{j=1}^{\chi} |\Psi_L^j\rangle \otimes |\Psi_R^j\rangle$ . Here, we consider generic  $|\Psi_R^j\rangle$  on the right, while  $|\Psi_L^j\rangle$  can be written as a one-site shift-invariant MPS of bond dimension  $\chi$  in terms of the three-leg tensor  $A_{jk}^{(a)}$ , where  $j = 0, 1, \dots, \chi-1$ . The matrices  $\{A^{(a)}\}$  act on the auxiliary Hilbert space  $\mathcal{H}_{\chi}$  spanned by the basis  $\{|j\rangle\}_{j=0}^{\chi-1}$ . Graphically, we can represent the folded tensor  $A$  as

$$\begin{array}{c} a, a' \\ \diagup \quad \diagdown \\ \text{---} \square \text{---} \\ \diagdown \quad \diagup \\ j, j' \end{array} \begin{array}{c} k, k' \\ \diagup \quad \diagdown \\ \text{---} \square \text{---} \\ \diagdown \quad \diagup \\ \end{array} = A_{jk}^{(a)} A_{j'k'}^{(a')*}, \quad (2)$$

such that the folded quantum state on the left region has the form

$$|\Psi_L^j\rangle\langle\Psi_L^{j'}| = \cdots \text{---} \square \text{---} \square \text{---} \square \text{---} \square \text{---} j, j'.$$

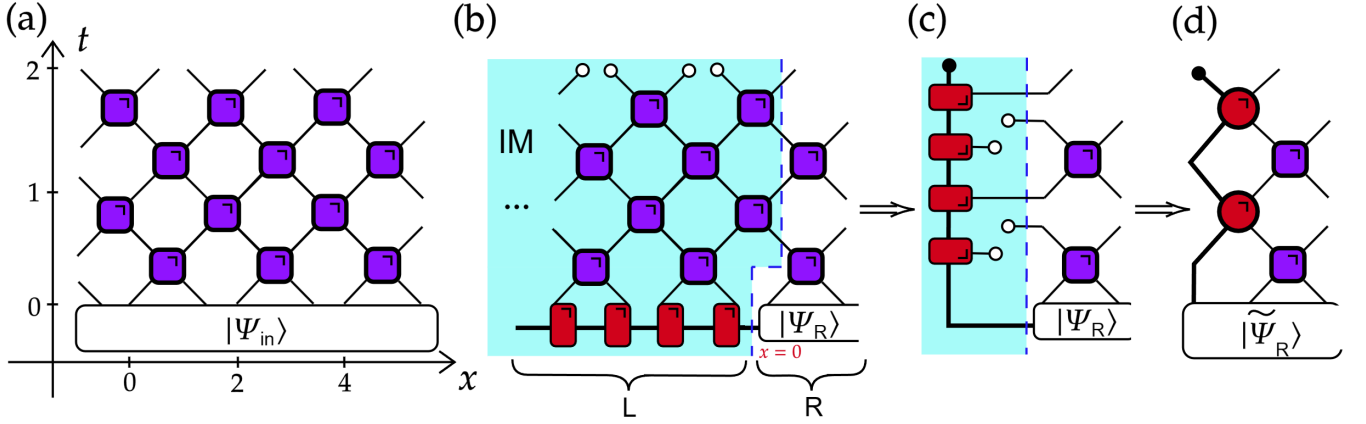


FIG. 1. Main results of this paper. Total time steps  $T = 2$ . (a) Tensor-network representation of a 1+1 D quantum circuit in the folded picture. The initial state  $|\Psi_{\text{in}}\rangle$  is evolved by applying four layers of two-site gates [purple squares, defined in Eq. (1)] in a brickwork architecture. (b) Illustration of the (left) influence matrix (IM). The system is initialized to a composite MPS over two regions: the left is a one-site shift invariant MPS [with local tensors in red, defined in Eq. (2)], and the right is a generic state. Thick lines correspond to the auxiliary Hilbert space. After attaching hollow dots on top outer legs in the left region, the tensor network in the light blue shaded region defines the influence matrix acting on the time slice (blue dotted line). (c) The exact influence matrix represented by MPS. (d) Open quantum system representation of the subsystem dynamics. Markovian property manifests when considering the joint dynamics of the ancilla in the auxiliary Hilbert space, and the subsystem. Two-site quantum channels are shown in red circles [defined in Eq. (5)].

We further assume that the MPS is injective and in the left-canonical form [19–21]:  $\sum_{a=0}^{q-1} A^{(a)\dagger} A^{(a)} = I_\chi$ , such that the left boundary condition becomes unimportant in the TL. Finally, we introduce the identity operators in the physical Hilbert space  $\mathcal{H}_q$  and the auxiliary Hilbert space  $\mathcal{H}_\chi$ , represented by the hollow and solid dot respectively:

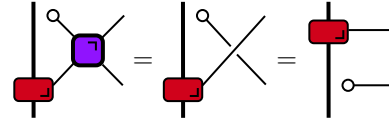
$$\begin{array}{c} \circ \\ a, a' \end{array} = \delta_{a,a'}, \quad \begin{array}{c} \bullet \\ j, j' \end{array} = \delta_{j,j'}. \quad (3)$$

*Exact influence matrix.*— We would like to explore the influence of an infinitely large system on its own subsystem. To this end, in our setup we take the region L be semi-infinite. Next, we trace out the region L after  $T$  time steps of evolution, and thus obtain the reduced density matrix on R:  $\rho_R(T) = \text{Tr}_L[\mathbb{U}^T |\Psi_{\text{in}}\rangle \langle \Psi_{\text{in}}| \mathbb{U}^{\dagger T}]$ . In Fig. 1(b), the partial trace operation after time evolution is carried out by attaching the identity operators to the outer legs in L. Consequently, the evolution of the subsystem on R can be expressed in terms of the internal dynamics  $\mathbb{U}_R$ , together with the action of a time non-local operator accounting for the temporal correlations in the left bath. As shown in Fig. 1(b), this operator lies on the multi-time Hilbert space, which is obtained by tensoring those local Hilbert spaces carried by the legs cut by the time slice. This operator is also referred to as the influence matrix (IM) [16].

We vectorize the IM to a quantum state in the doubled multi-time Hilbert space. Despite the class of dual unitary circuits and their generalizations which generate product-state IM [16, 22–28], examples of analytically tractable IM are limited to some exactly solvable models [29–31]. On the other hand, in generic quantum circuits, the long-time IM usually

becomes complicated, characterized by the bipartite entanglement entropy growing linearly with respect to the evolution time [16–18].

Here, we find a solvable condition of the IM for arbitrarily long time. The condition is an algebraic relation only involving the local unitary gate and the local MPS:

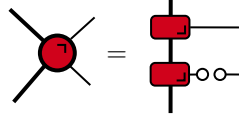


$$\text{Red Square} = \text{Red Square} \otimes \text{Purple Square} = \text{Red Square} \otimes \text{Red Circle} \quad (4)$$

Conceptually, this condition allows the tensor  $A$  to propagate freely in the quantum circuit along the diagonal direction. Indeed, the solvable condition can be viewed as a refined version of zipper conditions [32]. Previously, the zipper condition served as an *ansatz* to solve MPS influence matrices in integrable models [29, 31]. In contrast to those isolated examples, here we use the solvable condition as a criterion to construct generic non-integrable quantum circuits with exact influence matrices [33].

In Fig. 1(c), we directly present the exact form of IM under the solvable condition, while detailed derivations are put in [34]. An intuitive and heuristic picture is that, by tracing out the left region, the initial MPS is rotated by  $\pi/2$  and lies along the time slice, showing a novel manifestation of space-time duality. The IM is represented by a one-time-step shift-invariant MPS of bond dimension  $\chi^2$  with appropriate boundary conditions. The replicated element in the MPS is the fol-

lowing four-leg tensor:



$$(5)$$

This local tensor can be represented explicitly in terms of  $A$  [34], and replicates  $T$  times in the IM. At the lower boundary  $t = 0$ , the auxiliary leg is connected to the initial state in the region R; at the upper boundary  $t = T$ , the auxiliary Hilbert space is traced out.

*Exact Markovian subsystem dynamics.*— Next, we show that the exact IM gives rise to an emergent Markovian dynamics of the subsystem. In our constructions, as implied by the MPS representation, the IM is correlated in the time direction (when  $\chi > 1$ ), and thus the Markovian property seems to be lacking *in prior*. Nevertheless, Markovian property manifests when we consider the joint dynamics of an ancilla and the subsystem. The ancilla lives in the auxiliary Hilbert space  $\mathcal{H}_\chi$ . At  $t = 0$ , we prepare the joint system in the pure state  $|\Psi_R\rangle = \sum_{j=0}^{\chi-1} |j\rangle \otimes |\Psi_R^j\rangle$ , which gives the same subsystem reduced density matrix when tracing out the ancilla. Here  $\otimes$  denotes tensor products between the auxiliary and physical Hilbert space. As illustrated in Fig. 1(d), for each time step, the joint system is evolved by a layer of local gates, followed by a two-site quantum channel  $\mathcal{M}$  acting on the ancilla and the leftmost site:

$$\tilde{\rho}_R(t+1) = \mathcal{M}[\mathbb{U}_R \tilde{\rho}_R(t) \mathbb{U}_R^\dagger], \quad (6)$$

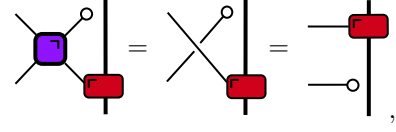
where  $\tilde{\rho}_R$  is the joint system density matrix. The dynamics of  $\tilde{\rho}_R$  is explicitly Markovian [35], where the state at the  $(t+1)$ th time step only depends on the state at  $t$ . The quantum channel  $\mathcal{M}$  is given by the four-leg tensor defined in Eq. (5), which can be written in the standard Kraus form [34, 36]:  $\mathcal{M}(\tilde{\rho}_R) = \sum_\mu K_\mu \tilde{\rho}_R K_\mu^\dagger$ , where the Kraus operators  $K_\mu$  are

$$K_\mu = K_{a,a'} = \sum_{b=0}^{q-1} A^{(b)} A^{(a)} \otimes (|b\rangle \langle a'|)_{x=0}. \quad (7)$$

Here  $a, a'$  run over 0 to  $q-1$ . Provided the Kraus-operator representation, the quantum channel  $\mathcal{M}$  is proved to be completely positive and trace-preserving (CPTP), which definitely justifies the Markovianity of joint dynamics [37]. The reduced density matrix on  $R$  can be obtained by tracing out the ancilla for each time step:  $\rho_R(t) = \text{Tr}_{\mathcal{H}_\chi}[\tilde{\rho}_R(t)]$ .

A few remarks are in order. First, we can prepare the left initial state in a Matrix Product Density Operator (MPDO), instead of a pure state in a MPS form. All the analysis works as well, except that the expressions of Kraus operators Eq. (7) should be slightly modified [34]. In this sense, we can unify dual-unitary circuits into our framework by choosing the identity operator as the  $\chi = 1$  local tensor in the left initial MPDO, and thus the solvable condition becomes dual-unitarity. Second, the left initial states can be extended to a certain class of

two-site shift-invariant MPS, while keeping the solvability of the influence matrix [34]. Third, due to the chiral structure in the solvable condition, it only allows efficient contractions of tensor networks from left to right, but not vice versa. However, by imposing an additional condition as follows:



$$(8)$$

contractions from the right are allowed as well. Quantum circuits equipped with two solvable conditions of opposite chirality lead to analytical expressions of more quantities, e.g. Rényi entropies dynamics [38]. In [34], we show that in this case the  $n$ th entanglement velocity  $v_E^{(n)}$  – asymptotic growing rate of the  $n$ th Rényi entropy ( $n > 1$ ) between two semi-infinite regions – is given by the leading eigenvalue  $\lambda_n$  of a certain quantum channel determined by  $A$ , i.e.,

$$v_E^{(n)} \equiv \lim_{t \rightarrow \infty} \frac{\ln(\text{Tr}[\rho_R^n(t)])}{t} = 2 \ln(\lambda_n). \quad (9)$$

Finally, we elaborate on the structure of the solvable condition Eq. (4), in preparation for discussing concrete examples. We begin with the simplest case of  $\chi = 1$  corresponding to the product state. We take the left initial state as  $\otimes_{x<0} |0\rangle_x$  for instance. The solvable condition Eq. (4) reads  $\text{Tr}_l[U(|0\rangle \langle 0| \otimes \rho)U^\dagger] = \text{Tr}[\rho] |0\rangle \langle 0|$ , which holds for any one-site density matrix  $\rho$ .  $\text{Tr}_l$  denotes tracing over the left site. When  $\chi > 1$ , the condition becomes  $\text{Tr}_l[U(|A_{jk}\rangle \langle A_{j'k'}| \otimes \rho)U^\dagger] = \text{Tr}[\rho] |A_{jk}\rangle \langle A_{j'k'}|$ , for all combinations of  $j, j', k, k'$ . Here the one-site MPS is defined as  $|A_{jk}\rangle = \sum_{a=0}^{q-1} A_{jk}^{(a)} |a\rangle$ . This suggests that, given the tensor  $A$ , the set of solutions of  $U$  under the solvable condition essentially depends on the Hilbert subspace  $\mathcal{H}_A$  spanned by  $\{|A_{jk}\rangle\}_{j,k=1}^\chi$ . More precisely, the solutions, up to one-site unitaries, should rely on the subspace dimension  $\tilde{q} = \dim(\mathcal{H}_A)$ . This is due to the isomorphism between different Hilbert subspaces with the same dimension. Notice that though distinct tensors  $A$  may yield the same  $\mathcal{H}_A$  (as will be shown later) and thus the same solutions, the resulting boundary quantum channels  $\mathcal{M}$  are still different. In the following, we will label the solutions of gates by  $q$  and  $\tilde{q}$ .

*Example I.*—In this and the next part, we will show that the solvable condition indeed leads to a wide range solutions of quantum circuits rather than being restricted. First, we present the solutions of  $q = 2, \tilde{q} = 1$ . For the reason demonstrated above, we can take a specific left initial state  $\otimes_{x<0} |0\rangle_x$ . In the context of MPS, the tensors are given by  $A^{(0)} = 1, A^{(1)} = 0$ , and thus  $\mathcal{H}_A = |0\rangle \langle 0|$ . We provide an exhaustive parameterization for the solutions [34]:

$$U = e^{i\phi} (u \otimes e^{-i\epsilon\sigma^3}) V[J] (e^{-i\eta\sigma^3} \otimes v), \quad (10)$$

where  $u, v \in \text{SU}(2)$ , and

$$V[J] = \exp \left[ -i \left( \frac{\pi}{4} \sigma^1 \otimes \sigma^1 + \frac{\pi}{4} \sigma^2 \otimes \sigma^2 + J \sigma^3 \otimes \sigma^3 \right) \right].$$

Here  $\sigma^\alpha$ ,  $\alpha = 1, 2, 3$  are standard Pauli matrices. This class of solutions coincides with those two-qubit circuits featuring in chiral solitons, which are dual-unitary [39].

Compared to those previously known solvable initial states for dual-unitary circuits [22], our findings suggest a new initial state  $(\otimes_{x<0} |0\rangle_x)$  allowing for a new exact influence matrix in the product-state form. The corresponding one-site quantum channel can be obtained by substituting the form of  $A$  into Eq. (7):  $\mathcal{M}[\rho_R] = (|0\rangle\langle 0|)_{x=0} \otimes \text{Tr}_{x=0}[\rho_R]$ . Hence, the left bath acts as the *boundary resetting* towards  $|0\rangle$ .

In addition, we point out that for the solutions Eq. (10), we can independently choose the one-site initial state as  $|0\rangle$  or  $|1\rangle$  while holding the solvability of the influence matrix.

*Example II.*— Next, we present a (non-exhaustive) parameterization for solutions with  $q = 4, \tilde{q} = 2$ , where  $\mathcal{H}_A$  is spanned by  $|0\rangle$  and  $|1\rangle$ :

$$U = e^{i\phi} W_2 S W_1 (I \otimes v). \quad (11)$$

Here  $v \in \text{SU}(4)$ ,  $S$  is the SWAP gate,  $W_{1,2}$  are one-site controlled gates:

$$W_{1,2} = \sum_{a=0}^3 f_{1,2}^{(a)} \otimes |a\rangle\langle a|, \quad (12)$$

where  $f_1^{(a)} = \begin{pmatrix} I_2 & 0 \\ 0 & g^{(a)} \end{pmatrix}$ ,  $g^{(a)} \in \text{SU}(2)$ , and  $f_2^{(a)} \in \text{SU}(4)$  for all  $a$ . The parameterization can be generalized to higher  $q$  and  $\tilde{q}$  with slight modifications:  $v \in \text{SU}(q)$ ,  $f_1^{(a)} = I_{\tilde{q}} \oplus g^{(a)}$  where  $g^{(a)} \in \text{SU}(q - \tilde{q})$ , and  $f_2^{(a)} \in \text{SU}(q)$ . Generally, these solutions form an overlapping but different set with dual-unitary circuits. An exception is when  $q - \tilde{q} = 0$  or  $1$ , where  $f_1^{(a)} = I_q$ ,  $W_1 = I_{q^2}$  and thus Eq. (11) is reduced to a subclass of dual-unitary gates [40, 41].

As an illustrative example, we report numerical results about the finite-size subsystem entanglement dynamics evolved by Eq. (11). For the left initial state, we choose the following  $\chi = 2$  MPS which spans  $\mathcal{H}_A$  with  $\tilde{q} = 2$ :  $A^{(0)} = \begin{pmatrix} \cos(\theta) & \sin(\theta) \\ 0 & 0 \end{pmatrix}$ ,  $A^{(1)} = \begin{pmatrix} 0 & 0 \\ -\sin(\theta) & \cos(\theta) \end{pmatrix}$ , and  $A^{(2,3)}$  are zero matrices. Here  $\theta \in (0, \frac{\pi}{4}]$ , which corresponds to the left initial state interpolating between the Greenberger-Horne-Zeilinger state and the cluster state [42, 43] of basis states  $|0\rangle$  and  $|1\rangle$ . As for the right region, we take the initial state as the simple product state  $|\Psi_R^j\rangle = \otimes_{x \geq 0} |2\rangle_x$ ,  $j = 0, 1$ , and thus the initial entanglement between regions L and R is zero. The right subsystem consists of four sites as shown faithfully in the left panel of Fig. 2. We construct the two-site gate  $U$  by randomly generating unitaries  $v, g^{(a)}$  and  $f_2^{(a)}$ .

Employing the influence matrix method, we can numerically keep track of the full time evolution of the joint system. The joint dynamics is generated by the Floquet operator Eq. (6), which is constituted by the unitary  $\mathbb{U}_R$  along with the boundary quantum channel  $\mathcal{M}$  given by Eq. (7). We compute the von Neumann entanglement entropy between two regions

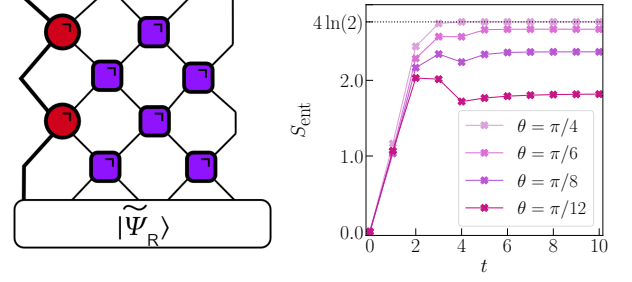


FIG. 2. Entanglement dynamics. Left panel: Illustration of the joint system, where the right region consists of four sites. Right panel: Growth of subsystem von Neumann entropies for different left initial MPS, which are characterized by the value of  $\theta$ . The right initial state and two-site gates are kept the same. The horizontal dotted line marked the maximal entropy  $4 \ln(2)$  approached by  $\theta = \pi/4$ .

as  $S_{\text{ent}}(t) = -\text{Tr}[\rho_R(t) \ln(\rho_R(t))]$ . We emphasize that the scenario here is basically different from that described by Eq. (9), where the size of  $R$  is infinitely large. Results for various values of  $\theta$  are depicted in the right panel of Fig. 2. Following a similar rate of linear growth in the early stage of evolution, the entropies approach the  $\theta$ -dependent steady values after finite time steps. Among the steady values, the maximal entropy  $4 \ln(2)$  is achieved by the case  $\theta = \pi/4$ , corresponding to the cluster state as the initial MPS. Notably, this maximal saturated entropy is still smaller than the maximum entropy allowed by the Hilbert space dimension of the right subsystem  $\ln(q^{L_R}) = 4 \ln(4)$ , which suggests violating the thermalization towards an infinite-temperature state. This observation hints at the existence of hidden conservation quantities, which demands further research.

*Conclusions.*— In summary, we have established a systematic approach towards constructions of non-integrable quantum circuits exhibiting exact Markovian subsystem dynamics. We introduced new principles beyond dual-unitary circuits allowing for closed-form influence matrices, which are formulated into the solvable condition on local unitary gates. Utilizing the tensor-network method, we demonstrated that the system acts as a time-local boundary quantum channel on the subsystem, thus inducing exact Markovian dynamics. Our constructions have unveiled a novel space-time duality between initial state MPS of the system and boundary quantum channels acting on the reduced subsystem.

Our work opens up many avenues for future research, such as the introduction of measurements [44] and dissipation [45], generalizations to different architectures [41, 46] and higher spatial dimensions [24, 47, 48]. The exact influence matrices also provide valuable analytical tools for studying rich phenomena in quantum many-body dynamics, including quantum chaos [49] and deep thermalization [44, 50, 51].

Furthermore, our findings on the exact subsystem Markovian property could provide fresh insights into the fundamental understanding of the Markovian approximation. Typically, in isolated quantum many-body systems, tracing out the



rest of degrees of freedom usually yields non-Markovian subsystem dynamics [52]. A valid Markovian description usually resorts to weak system-bath coupling and the separation of timescales [53, 54]. In contrast, in our construction the Markovian property emerges non-perturbatively as a consequence of the solvable condition, which only involves properties of local gates and initial states. Understanding deep relations between these solvable quantum circuits and the Markovian approximation remains an intriguing area for further exploration.

*Acknowledgment.*— We thank Tianci Zhou for helpful discussions. This work was supported by the National Natural Science Foundation of China (Grants No. 12125405), and National Key R&D Program of China (No. 2023YFA1406702).

- 
- [1] J. M. Deutsch, “Quantum statistical mechanics in a closed system,” *Phys. Rev. A* **43**, 2046 (1991).
  - [2] M. Srednicki, “Chaos and quantum thermalization,” *Phys. Rev. E* **50**, 888 (1994).
  - [3] M. Rigol, V. Dunjko, and M. Olshanii, “Thermalization and its mechanism for generic isolated quantum systems,” *Nature* **452**, 854 (2008).
  - [4] M. A. Cazalilla and M. Rigol, “Focus on dynamics and thermalization in isolated quantum many-body systems,” *New J. Phys.* **12**, 055006 (2010).
  - [5] A. Polkovnikov, K. Sengupta, A. Silva, and M. Vengalattore, “Colloquium: Nonequilibrium dynamics of closed interacting quantum systems,” *Rev. Mod. Phys.* **83**, 863 (2011).
  - [6] B. Sutherland, *Beautiful models: 70 years of exactly solved quantum many-body problems* (World Scientific, 2004).
  - [7] R. Nandkishore and D. A. Huse, “Many-body localization and thermalization in quantum statistical mechanics,” *Annu. Rev. Condens. Matter Phys.* **6**, 15 (2015).
  - [8] D. A. Abanin, E. Altman, I. Bloch, and M. Serbyn, “Colloquium: Many-body localization, thermalization, and entanglement,” *Rev. Mod. Phys.* **91**, 021001 (2019).
  - [9] M. Serbyn, D. A. Abanin, and Z. Papić, “Quantum many-body scars and weak breaking of ergodicity,” *Nat. Phys.* **17**, 675 (2021).
  - [10] S. Moudgalya, B. A. Bernevig, and N. Regnault, “Quantum many-body scars and hilbert space fragmentation: A review of exact results,” *Rep. Prog. Phys.* **85**, 086501 (2022).
  - [11] A. Chandran, T. Iadecola, V. Khemani, and R. Moessner, “Quantum many-body scars: A quasiparticle perspective,” *Annu. Rev. Condens. Matter Phys.* **14** (2022).
  - [12] M. C. Bañuls, M. B. Hastings, F. Verstraete, and J. I. Cirac, “Matrix product states for dynamical simulation of infinite chains,” *Phys. Rev. Lett.* **102**, 240603 (2009).
  - [13] A. Müller-Hermes, J. I. Cirac, and M. C. Bañuls, “Tensor network techniques for the computation of dynamical observables in one-dimensional quantum spin systems,” *New J. Phys.* **14**, 075003 (2012).
  - [14] M. B. Hastings and R. Mahajan, “Connecting entanglement in time and space: Improving the folding algorithm,” *Phys. Rev. A* **91**, 032306 (2015).
  - [15] M. Frías-Pérez and M. C. Bañuls, “Light cone tensor network and time evolution,” *Phys. Rev. B* **106**, 115117 (2022).
  - [16] A. Leroose, M. Sonner, and D. A. Abanin, “Influence matrix approach to many-body floquet dynamics,” *Phys. Rev. X* **11**, 021040 (2021).
  - [17] M. Sonner, A. Leroose, and D. A. Abanin, “Influence functional of many-body systems: Temporal entanglement and matrix-product state representation,” *Ann. Phys.* **435**, 168677 (2021), special issue on Philip W. Anderson.
  - [18] A. Foligno, T. Zhou, and B. Bertini, “Temporal entanglement in chaotic quantum circuits,” *Phys. Rev. X* **13**, 041008 (2023).
  - [19] D. Perez-Garcia, F. Verstraete, M. M. Wolf, and J. I. Cirac, “Matrix product state representations,” *Quantum Info. Comput.* **7**, 401–430 (2007).
  - [20] G. Vidal, “Efficient classical simulation of slightly entangled quantum computations,” *Phys. Rev. Lett.* **91**, 147902 (2003).
  - [21] S. R. White and A. E. Feiguin, “Real-time evolution using the density matrix renormalization group,” *Phys. Rev. Lett.* **93**, 076401 (2004).
  - [22] B. Bertini, P. Kos, and T. c. v. Prosen, “Exact correlation functions for dual-unitary lattice models in  $1+1$  dimensions,” *Phys. Rev. Lett.* **123**, 210601 (2019).
  - [23] L. Piroli, B. Bertini, J. I. Cirac, and T. c. v. Prosen, “Exact dynamics in dual-unitary quantum circuits,” *Phys. Rev. B* **101**, 094304 (2020).
  - [24] C. Jonay, V. Khemani, and M. Ippoliti, “Triunitary quantum circuits,” *Phys. Rev. Res.* **3**, 043046 (2021).
  - [25] X.-H. Yu, Z. Wang, and P. Kos, “Hierarchical generalization of dual unitarity,” *Quantum* (2023), 10.22331/q-2024-02-20-1260.
  - [26] B. Bertini, C. D. Fazio, J. P. Garrahan, and K. Klobas, “Exact quench dynamics of the floquet quantum east model at the deterministic point,” *arXiv:2310.06128* (2023).
  - [27] C. Liu and W. W. Ho, “Solvable entanglement dynamics in quantum circuits with generalized dual unitarity,” *arXiv:2312.12239* (2023).
  - [28] A. Foligno, P. Kos, and B. Bertini, “Quantum information spreading in generalised dual-unitary circuits,” *arXiv:2312.02940* (2023).
  - [29] K. Klobas, B. Bertini, and L. Piroli, “Exact thermalization dynamics in the “rule 54” quantum cellular automaton,” *Phys. Rev. Lett.* **126**, 160602 (2021).
  - [30] A. Leroose, M. Sonner, and D. A. Abanin, “Scaling of temporal entanglement in proximity to integrability,” *Phys. Rev. B* **104**, 035137 (2021).
  - [31] G. Giudice, G. Giudici, M. Sonner, J. Thoenness, A. Leroose, D. A. Abanin, and L. Piroli, “Temporal entanglement, quasiparticles, and the role of interactions,” *Phys. Rev. Lett.* **128**, 220401 (2022).
  - [32] J. Haegeman and F. Verstraete, “Diagonalizing transfer matrices and matrix product operators: A medley of exact and computational methods,” *Annu. Rev. Condens. Matter Phys.* **8**, 355 (2017).
  - [33] We would like to draw a loose analogy between the relationship of zipper conditions and our solvable condition, with that of the Bethe ansatz and Yang-Baxter equations. The Bethe ansatz was initially proposed to solve the energies and eigenstates of the 1D Heisenberg spin chain, while Yang-Baxter equations capture the crucial point (factorizable scattering amplitudes) and the solutions give rise to a wide class of Bethe-ansatz solvable models. In a similar vein, zipper conditions were used to solve specific models, while our solvable condition provides a systematic approach to constructing solvable quantum circuits.
  - [34] See the Supplementary Materials at [URL will be inserted by publisher] for diagrammatic derivations of the exact influence matrix, solvable two-site shift-invariant initial MPS, derivations of the Kraus representation for the boundary quantum channel (with MPS and MPDO initial states), analytically calculating

- Rényi entropies dynamics for infinitely large subsystems, and more details on the examples of  $q = 2$ ,  $\tilde{q} = 1$  and 2.
- [35] This step can be traced back to the Pseudo-mode approach, by incorporating random variables or collective coordinates into the non-Markovian system to create the time-local joint dynamics [55–59]. This approach has been generalized to various scenarios of open quantum systems [60–65].
  - [36] M. A. Nielsen and I. L. Chuang, *Quantum computation and quantum information* (Cambridge university press, 2010).
  - [37] H.-P. Breuer, E.-M. Laine, J. Piilo, and B. Vacchini, “Colloquium: Non-markovian dynamics in open quantum systems,” *Rev. Mod. Phys.* **88**, 021002 (2016).
  - [38] B. Bertini, K. Klobas, V. Alba, G. Lagnese, and P. Calabrese, “Growth of rényi entropies in interacting integrable models and the breakdown of the quasiparticle picture,” *Phys. Rev. X* **12**, 031016 (2022).
  - [39] B. Bertini, P. Kos, and T. Prosen, “Operator entanglement in local quantum circuits ii: Solitons in chains of qubits,” *SciPost Phys.* **8**, 068 (2020).
  - [40] M. Borsi and B. Pozsgay, “Construction and the ergodicity properties of dual unitary quantum circuits,” *Phys. Rev. B* **106**, 014302 (2022).
  - [41] T. Prosen, “Many-body quantum chaos and dual-unitarity round-a-face,” *Chaos* **31** (2021), 10.1063/5.0056970.
  - [42] R. Raussendorf and H. J. Briegel, “A one-way quantum computer,” *Phys. Rev. Lett.* **86**, 5188 (2001).
  - [43] F. Verstraete and J. I. Cirac, “Valence-bond states for quantum computation,” *Phys. Rev. A* **70**, 060302 (2004).
  - [44] P. W. Claeys, M. Henry, J. Vicary, and A. Lamacraft, “Exact dynamics in dual-unitary quantum circuits with projective measurements,” *Phys. Rev. Res.* **4**, 043212 (2022).
  - [45] P. Kos and G. Styliaris, “Circuits of space and time quantum channels,” *Quantum* **7**, 1020 (2023).
  - [46] P. W. Claeys, A. Lamacraft, and J. Vicary, “From dual-unitary to biunitary: a 2-categorical model for exactly-solvable many-body quantum dynamics,” *arXiv:2302.07280* (2023).
  - [47] R. Suzuki, K. Mitarai, and K. Fujii, “Computational power of one- and two-dimensional dual-unitary quantum circuits,” *Quantum* **6**, 631 (2022).
  - [48] R. M. Milbradt, L. Scheller, C. Abmus, and C. B. Mendl, “Ternary unitary quantum lattice models and circuits in  $2 + 1$  dimensions,” *Phys. Rev. Lett.* **130**, 090601 (2023).
  - [49] B. Bertini, P. Kos, and T. c. v. Prosen, “Exact spectral form factor in a minimal model of many-body quantum chaos,” *Phys. Rev. Lett.* **121**, 264101 (2018).
  - [50] W. W. Ho and S. Choi, “Exact emergent quantum state designs from quantum chaotic dynamics,” *Phys. Rev. Lett.* **128**, 060601 (2022).
  - [51] M. Ippoliti and W. W. Ho, “Dynamical purification and the emergence of quantum state designs from the projected ensemble,” *PRX Quantum* **4**, 030322 (2023).
  - [52] H.-P. Breuer and F. Petruccione, *The theory of open quantum systems* (Oxford University Press, USA, 2002).
  - [53] E. B. Davies, “Markovian master equations,” *Communications in mathematical Physics* **39**, 91 (1974).
  - [54] G. Lindblad, “On the generators of quantum dynamical semigroups,” *Communications in Mathematical Physics* **48**, 119 (1976).
  - [55] A. Imamoglu, “Stochastic wave-function approach to non-markovian systems,” *Phys. Rev. A* **50**, 3650 (1994).
  - [56] B. M. Garraway, “Nonperturbative decay of an atomic system in a cavity,” *Phys. Rev. A* **55**, 2290 (1997).
  - [57] L. Mazzola, S. Maniscalco, J. Piilo, K.-A. Suominen, and B. M. Garraway, “Pseudomodes as an effective description of memory: Non-markovian dynamics of two-state systems in structured reservoirs,” *Phys. Rev. A* **80**, 012104 (2009).
  - [58] J. Iles-Smith, N. Lambert, and A. Nazir, “Environmental dynamics, correlations, and the emergence of noncanonical equilibrium states in open quantum systems,” *Phys. Rev. A* **90**, 032114 (2014).
  - [59] F. Mascherpa, A. Smirne, A. D. Somoza, P. Fernández-Acebal, S. Donadi, D. Tamascelli, S. F. Huelga, and M. B. Plenio, “Optimized auxiliary oscillators for the simulation of general open quantum systems,” *Phys. Rev. A* **101**, 052108 (2020).
  - [60] S. Kretschmer, K. Luoma, and W. T. Strunz, “Collision model for non-markovian quantum dynamics,” *Phys. Rev. A* **94**, 012106 (2016).
  - [61] S. Campbell, F. Ciccarello, G. M. Palma, and B. Vacchini, “System-environment correlations and markovian embedding of quantum non-markovian dynamics,” *Phys. Rev. A* **98**, 012142 (2018).
  - [62] D. Tamascelli, A. Smirne, S. F. Huelga, and M. B. Plenio, “Nonperturbative treatment of non-markovian dynamics of open quantum systems,” *Phys. Rev. Lett.* **120**, 030402 (2018).
  - [63] I. A. Luchnikov, S. V. Vintskevich, D. A. Grigoriev, and S. N. Filippov, “Machine learning non-markovian quantum dynamics,” *Phys. Rev. Lett.* **124**, 140502 (2020).
  - [64] S. N. Filippov and I. A. Luchnikov, “Collisional open quantum dynamics with a generally correlated environment: Exact solvability in tensor networks,” *Phys. Rev. A* **105**, 062410 (2022).
  - [65] S. Flannigan, F. Damanet, and A. J. Daley, “Many-body quantum state diffusion for non-markovian dynamics in strongly interacting systems,” *Phys. Rev. Lett.* **128**, 063601 (2022).

# Supplementary Materials for: Exact Markovian dynamics in quantum circuits

He-Ran Wang,<sup>1</sup> Xiao-Yang Yang,<sup>1,2</sup> and Zhong Wang<sup>1</sup>

<sup>1</sup>*Institute for Advanced Study, Tsinghua University, Beijing 100084, People's Republic of China*

<sup>2</sup>*Department of Physics, Tsinghua University, Beijing 100084, People's Republic of China*

## I. EXACT INFLUENCE MATRIX FROM THE SOLVABLE CONDITION

In this section, we derive the exact influence matrix in the Matrix Product State (MPS) representation from the solvable condition. We present the proof from two directions: First, we perform straightforward contractions on the 1+1D tensor network to obtain the influence matrix on the time slice (Sec. **IA**); Second, we show that the obtained influence matrix is indeed the fixed point of the spatial transfer matrix (Sec. **IB**). All the calculations are shown in diagrammatic representations.

### A. Contractions of the tensor network

We summarize the procedure of contractions in Fig. **S1**. We begin with the tensor network representing the traced time-evolved state in the region  $L$ , as depicted in Fig. **S1(a)** [see also Fig. 1(b) in the main text]. In the first step, we apply the following two local rules: the unitarity of local gates

$$\text{Diagram: A purple square with four legs (two horizontal, two vertical) and two small circles on top} = \text{Diagram: Two vertical lines} \quad (S1)$$

and the left-canonical condition of the MPS

$$\text{Diagram: A red square with a horizontal line on the left, a vertical line on the right, and a small circle on top} = \text{Diagram: A horizontal line} \quad (S2)$$

The two local rules allow efficient contractions of the tensor network within the lightcone. More specifically, all the tensors in the space-time region  $2t - x > 2T$  are reduced to the identities lying along the edge of the lightcone  $2t - x = 2T$ , as shown in Fig. **S1(b)**. Notice that this step is independent of the solvable condition, and thus is universal for brickwork quantum circuits.

Next, we employ the solvable condition to achieve further simplifications:

$$\text{Diagram: A purple square with a red square on its left leg} = \text{Diagram: A purple square with a red square on its right leg} = \text{Diagram: A red square with a small circle on top} \quad (S3)$$

For instance, we can apply this condition on the tensor located at the lower-left corner in Fig. **S1(b)** (circled by the grey dotted line), which gives

$$\text{Diagram: A purple square with a red square on its left leg and a red square on its right leg} = \text{Diagram: A red square with a diagonal line and a small circle on top} \quad (S4)$$

We perform such contractions along the edge of the lightcone  $2t - x = 2T$  to shift the identities to the next edge, as shown in Fig. **S1(c)**. By repeating this “lightcone decimation” procedure for  $T$  times, we arrive at the closed-form influence matrix with outer legs across the time slice, the same as Fig. 1(c) in the main text.

The contractions imply a novel manifestation of *space-time duality* between the initial state MPS and the influence matrix: The local MPS located at an even site  $x$  in the initial state exactly corresponds to the local MPS in the influence matrix at  $t = -x/2$ .

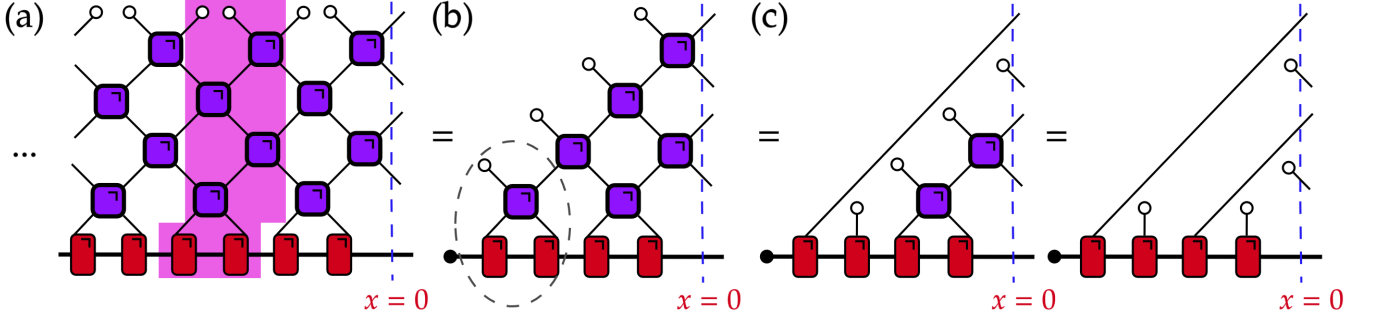


FIG. S1. Contractions of the tensor network. Total time steps  $T = 2$ . The red shaded region in (a) is a layer of spatial transfer matrix. From (a) to (b), we use two local rules Eq. (S1) and Eq. (S2) to contract all the tensors within the lightcone. From (b) to (c), we proceed contractions using the solvable condition Eq. (S3).

### B. Fixed point condition

In quantum circuits respecting shift invariance in the space direction, the influence matrix of a global system can be identified as the fixed point of the spatial transfer matrix [1–4]. In our brickwork architecture which is two-site shift invariant, the spatial transfer matrix [visualized in red shaded region in Fig. S1(a)] involves two layers. To verify the fixed point condition, we contract the spatial transfer matrix with the obtained influence matrix from the right hand side, which yields

(S5)

In the first two equalities, we only exploit the solvable condition Eq. (S3), while the last equality is based on the left-canonical form [Eq. (S2)]. We have proved that the MPS influence matrix is the fixed point of the spatial transfer matrix.

### C. Two-site shift-invariant initial MPS

Here we discuss a class of two-site shift-invariant initial MPS which also leads to exact influence matrices under the solvable condition Eq. (S3). We consider the following left initial state in the alternating MPS form:

$$\cdots \text{---} \text{red tensor} \text{---} \text{blue tensor} \text{---} \text{red tensor} \text{---} \text{blue tensor} \text{---} j, j', \quad (S6)$$

where the new tensor in blue is defined as

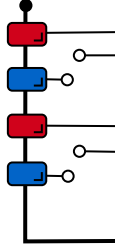
$$j, j' \text{---} \text{blue tensor} \text{---} k, k' = B_{jk}^{(a)} B_{j'k'}^{(a')*}. \quad (S7)$$

In such an initial state, the even (odd) site is associated with the tensor  $A(B)$  (remind that we have set the leftmost site of the right region to  $x = 0$ ). In this case, the matrices  $A^{(a)}$  and  $B^{(b)}$  are not necessarily square matrices; they can be  $\chi \times \chi'$  and  $\chi' \times \chi$ , respectively. We still require that the MPS is injective and in the left-canonical form, which reads

$$\sum_{a,b=0}^{q-1} (A^{(a)} B^{(b)})^\dagger A^{(a)} B^{(b)} = I_\chi. \quad (S8)$$



Notice that the solvable condition Eq. (S3) we imposed is irrelevant of the tensor  $B$ . Following the same approach presented in Fig. S1, one can show that tracing out the left region results in the following influence matrix (an example for  $t = 2$ ):

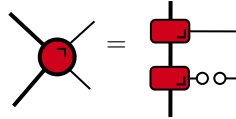


(S9)

## II. BOUNDARY QUANTUM CHANNEL

### A. Kraus-operator representation

In this subsection, we derive the concrete expressions of the time-local boundary quantum channel defined by



(S10)

The action of quantum channel can be directly read out from the diagram following the down-to-up direction:

$$\mathcal{M}(\tilde{\rho}_R) = \sum_{b,b'=0}^{q-1} A^{(b)} \left( \sum_{a=0}^{q-1} A^{(a)} \text{Tr}_{x=0}[\tilde{\rho}_R] A^{(a)\dagger} \right) A^{(b')\dagger} \bigotimes (|b\rangle \langle b'|)_{x=0}. \quad (\text{S11})$$

We shall bring this expression into the standard Kraus representation. To this end, we rewrite the trace operation over the Hilbert space at  $x = 0$  as  $\text{Tr}_{x=0}[\tilde{\rho}_R] = \sum_{a'=0}^{q-1} \langle a' | \tilde{\rho}_R | a' \rangle$ . Plugging this decomposition into Eq. (S11) leads to

$$\mathcal{M}(\tilde{\rho}_R) = \sum_{a,a',b,b'=0}^{q-1} [A^{(b)} A^{(a)} \bigotimes (|b\rangle \langle a'|)_{x=0}] \tilde{\rho}_R [A^{(a)\dagger} A^{(b')\dagger} \bigotimes (|a'\rangle \langle b'|)_{x=0}]. \quad (\text{S12})$$

The summation is over  $a, a', b, b'$ . However, notice that the index  $b$  and  $b'$  appear in different sides of  $\tilde{\rho}_R$  independently. Therefore, we can recast the operators on the single side of  $\tilde{\rho}_R$  into the Kraus operator by summing over  $b$ :

$$K_{a,a'} = \sum_{b=0}^{q-1} A^{(b)} A^{(a)} \bigotimes (|b\rangle \langle a'|)_{x=0}. \quad (\text{S13})$$

Consequently, Eq. (S11) becomes  $\mathcal{M}(\tilde{\rho}_R) = \sum_{a,a'=0}^{q-1} K_{a,a'} \tilde{\rho}_R K_{a,a'}^\dagger$ . We can check the trace-preserving property of Kraus operators as follows:

$$\begin{aligned}
\sum_{a,a'=0}^{q-1} K_{a,a'}^\dagger K_{a,a'} &= \sum_{a,a',b,b'=0}^{q-1} A^{(a)\dagger} A^{(b)\dagger} A^{(b')} A^{(a)} \bigotimes |a'\rangle \langle b| b'\rangle \langle a'| \\
&= \left( \sum_{a,b,b'=0}^{q-1} \delta_{b,b'} A^{(a)\dagger} A^{(b)\dagger} A^{(b')} A^{(a)} \right) \bigotimes \left( \sum_{a'=0}^{q-1} |a'\rangle \langle a'| \right) \\
&= \sum_{a=0}^{q-1} A^{(a)\dagger} \left( \sum_{b=0}^{q-1} A^{(b)\dagger} A^{(b)} \right) A^{(a)} \bigotimes I_q \\
&= \sum_{a=0}^{q-1} A^{(a)\dagger} A^{(a)} \bigotimes I_q = I_\chi \bigotimes I_q.
\end{aligned} \tag{S14}$$

Here the equation  $\sum_{a=0}^{q-1} A^{(a)\dagger} A^{(a)} = I_\chi$  comes from the left-canonical condition.

Similarly, for the case of two-site shift invariant initial MPS described in Sec. IC, the Kraus operators are given by

$$K_{a,a'} = \sum_{b=0}^{q-1} A^{(b)} B^{(a)} \bigotimes (|b\rangle \langle a'|)_{x=0}. \quad (\text{S15})$$

### B. Mixed initial states

Here, we generalize the quantum channel expression to the mixed initial states admitting Matrix Product Density Operator (MPDO) representation. We further impose the locally purified condition, that is, the MPDO can be purified to a MPS with a local purifying auxiliary system [5, 6]. MPDO with the locally purified condition is also termed as the Locally Purified Density Operator (LPDO). In this case, the three-leg local tensor  $\mathcal{A}$  reads

$$j, j' \text{ --- } \text{red square} \text{ --- } k, k' = \mathcal{A}_{jk, j'k'}^{(a, a')} = \sum_{\gamma=0}^{D-1} A_{jk}^{(a, \gamma)} A_{j'k'}^{(a', \gamma)*}, \quad (\text{S16})$$

where  $\gamma$  is the auxiliary index corresponding to the local purification space of dimension  $D$ . In this context, the left-canonical condition is formulated as

$$\sum_{\gamma=0}^{D-1} \sum_{a=0}^{q-1} A^{(a, \gamma)\dagger} A^{(a, \gamma)} = I_\chi. \quad (\text{S17})$$

For the  $D = 1$  case, the LPDO is reduced to the pure-state MPS studied in the main text.

The LPDO corresponds to the quantum channel

$$\mathcal{M}(\tilde{\rho}_R) = \sum_{\gamma'=0}^{D-1} \sum_{b, b'=0}^{q-1} A^{(b, \gamma')} \left( \sum_{\gamma=0}^{D-1} \sum_{a=0}^{q-1} A^{(a, \gamma)} \text{Tr}_{x=0}[\tilde{\rho}_R] A^{(a, \gamma)\dagger} \right) A^{(b', \gamma')\dagger} \bigotimes (|b\rangle \langle b'|)_{x=0}. \quad (\text{S18})$$

Following the similar analysis, we can extract the Kraus operators from the quantum channel expression:

$$K_{(a\gamma, a'\gamma')} = \sum_{b=0}^{q-1} A^{(b, \gamma')} A^{(a, \gamma)} \bigotimes (|b\rangle \langle a'|)_{x=0}. \quad (\text{S19})$$

### III. RÉNYI ENTROPIES DYNAMICS

Here, we preform tensor-network contractions to obtain analytical expressions for the time-evolved Rényi entropies  $S_R^{(n)}(t) = \ln(\text{Tr}[\rho_R^n(t)])/(1-n)$ . We work in the space-time regime where  $\text{size(L)}$  and  $\text{size(R)}$  are larger than  $2t$ , such that the most efficient contractions of tensor networks from both sides are allowed. This regime corresponds to the early-stage growth of entanglement. Due to the presence of the strict light cone in brickwork architectures, we can extend  $\text{size(L)}$  and  $\text{size(R)}$  to infinite, without altering the results. As demonstrated in the main text, we impose both solvable conditions with opposite chirality, quoted as below:

$$\begin{array}{c} \text{red square} \\ \text{---} \end{array} \begin{array}{c} \text{blue square} \\ \text{---} \end{array} = \begin{array}{c} \text{red square} \\ \text{---} \end{array} \begin{array}{c} \text{blue square} \\ \text{---} \end{array}, \quad \begin{array}{c} \text{blue square} \\ \text{---} \end{array} \begin{array}{c} \text{red square} \\ \text{---} \end{array} = \begin{array}{c} \text{blue square} \\ \text{---} \end{array} \begin{array}{c} \text{red square} \\ \text{---} \end{array}. \quad (\text{S20})$$

Meanwhile, we choose the initial state as the homogeneous, one-site shift invariant MPS with local tensor  $A$ . To dispense with the influence of boundary conditions, we further assume that the MPS is in the left- and right-canonical form:  $\sum_{a=0}^{q-1} A^{(a)\dagger} A^{(a)} = \sum_{a=0}^{q-1} A^{(a)} A^{(a)\dagger} = I_\chi$ .

In Sec. III A, we introduce basic notions of the multi-folded representation, which are needed to present  $\text{Tr}[\rho_R^n(t)]$  graphically. Subsequently, we apply the solvable conditions to contract the tensor network in Sec. III B, and establish the correspondence between the  $n$ th Rényi entropy at the time step  $t$  and the repeated  $2t$ -time action of a certain quantum channel, which is not trace-preserving. Thus, this correspondence provides an operational approach to accurately calculating the initial growing rate of the entanglement.

### A. Multi-folded representations

In the main text, we have adopted the folded representation to represent the time-evolved state by a single patch of tensor network, i.e. Fig. 1(a) in the main text. Here, in order to represent the  $n$ th power of the state, we introduce the  $n$ -folded representation for unitary gates and MPS as follows:

$$\text{[Diagram: A square with four lines extending from its corners, representing a unitary gate]} = (U \otimes U^*)^{\otimes n}, \quad \text{[Diagram: A green rectangle with two lines extending from its top and bottom, representing an MPS]} = (A \otimes A^*)^{\otimes n}. \quad (\text{S21})$$

Consequently, we can represent the  $n$ -replica of a time-evolved pure state as below,  $t = 2$  for example:

$$(|\Psi(t)\rangle\langle\Psi(t)|)^{\otimes n} = \text{[Diagram: A tensor network representing the } n\text{-replica of a time-evolved pure state. It consists of a grid of orange squares (unitaries) and a row of green rectangles (MPS) at the bottom. The grid is 4 rows high and 6 columns wide. The bottom row of green rectangles is connected to the grid by lines. The top and side lines of the grid are open.]}$$
(S22)

Then we trace out the degrees of freedom in L to obtain  $\rho_R(t)^{\otimes n}$ . In the  $n$ -folded representation, the tracing operation manifests as a certain contraction on each site:  $\delta_{a_1, a'_1} \cdots \delta_{a_n, a'_n}$ , where  $a_m$  and  $a'_m$  correspond to the forward and backward branches on a single-site Hilbert space in the  $m$ th replica, respectively. We still use the hollow dot to represent such a contraction operator. The  $n$ -replica reduced density matrix is represented as:

$$\rho_R(t)^{\otimes n} = \text{[Diagram: A tensor network for the reduced density matrix. It is similar to (S22) but with a dashed line labeled 'L' above the top row of orange squares, indicating a contraction. The top row of orange squares is now connected to the bottom row of green rectangles by lines. The top and side lines of the grid are open. The diagram is labeled 'L' and 'R' above the dashed line.]}$$
(S23)

The next step is to inserting a certain permutation operator  $\mathbb{P}_n$  and trace out R:  $\text{Tr}[\rho_R^n(t)] = \text{Tr}[\mathbb{P}_n \rho_R(t)^{\otimes n}]$  [7]. Notably, this operation is equivalent to conducting the following contraction on each site:  $\delta_{a'_1, a_2} \delta_{a'_2, a_3} \cdots \delta_{a'_{n-1}, a_n} \delta_{a'_n, a_1}$ . We use the hollow diamond to represent this contraction:

$$\text{[Diagram: A hollow diamond shape with four lines extending from its corners, representing a contraction operator]} = \delta_{a'_1, a_2} \cdots \delta_{a'_n, a_1}. \quad (\text{S24})$$

Therefore, we have:

$$\text{Tr}[\rho_R^n(t)] = \text{[Diagram: A tensor network for the trace of the } n\text{-replica reduced density matrix. It is similar to (S23) but with a dashed line labeled 'R' above the top row of orange squares, indicating a contraction. The top row of orange squares is now connected to the bottom row of green rectangles by lines. The top and side lines of the grid are open. The diagram is labeled 'L' and 'R' above the dashed line.]}$$
(S25)



#### IV. $q = 2$ SOLUTIONS FOR THE SOLVABLE CONDITION

In this section we focus on solving the two-qubit gates fulfilling the solvable condition. The solutions for both  $\tilde{q} = 1$  and  $\tilde{q} = 2$  are covered by the dual-unitary gates [8]. For  $\tilde{q} = 1$ , we show that the solutions feature in chiral solitons [9], given by Eq. (9) in the main text (Sec. IV B). On the other hand, the  $\tilde{q} = 2$  solutions are SWAP gates dressed by single-site unitaries (Sec. IV C).

##### A. Preliminary: two-qubit gates

To begin with, notice that every two-qubit unitary gate can be parameterized as [10–12]:

$$U = e^{i\phi}(u_+ \otimes u_-)V[J_1, J_2, J_3](v_- \otimes v_+), \quad (\text{S33})$$

where  $u_{\pm}, v_{\pm} \in \text{SU}(2)$ , and

$$V[J_1, J_2, J_3] = \exp[-i(J_1\sigma^1 \otimes \sigma^1 + J_2\sigma^2 \otimes \sigma^2 + J_3\sigma^3 \otimes \sigma^3)]. \quad (\text{S34})$$

Since increasing any  $J_{\alpha}$  by  $\frac{\pi}{2}$  is equivalent to applying a tensor product of two single-site unitaries which can be absorbed into  $u_{\pm}, v_{\pm}$ , we can restrict the range of  $J_{\alpha}$  within  $[0, \frac{\pi}{2})$ . The matrix  $V[J_1, J_2, J_3]$  can also be written on the Pauli basis [9]:

$$V[J_1, J_2, J_3] = \sum_{\alpha=0}^3 V_{\alpha}(J_1, J_2, J_3)\sigma^{\alpha} \otimes \sigma^{\alpha}, \quad (\text{S35})$$

where the identity has been included in the Pauli matrices as  $\sigma^0 = I_2$ . Here  $V_{\alpha}(J_1, J_2, J_3)$  are some complex-valued coefficients:

$$\begin{aligned} V_0(J_1, J_2, J_3) &= \cos(J_1) \cos(J_2) \cos(J_3) - i \sin(J_1) \sin(J_2) \sin(J_3), \\ V_1(J_1, J_2, J_3) &= \cos(J_1) \sin(J_2) \sin(J_3) - i \sin(J_1) \cos(J_2) \cos(J_3), \\ V_2(J_1, J_2, J_3) &= \sin(J_1) \cos(J_2) \sin(J_3) - i \cos(J_1) \sin(J_2) \cos(J_3), \\ V_3(J_1, J_2, J_3) &= \sin(J_1) \sin(J_2) \cos(J_3) - i \cos(J_1) \cos(J_2) \sin(J_3). \end{aligned} \quad (\text{S36})$$

We adopt this parameterization and identify the constraints on all the parameters ( $u_{\pm}, v_{\pm}$  and  $J_{1,2,3}$ ) under the solvable condition.

##### B. $q = 2, \tilde{q} = 1$

Here we choose the one-site state to be  $|0\rangle$ , that is,  $\mathcal{H}_A = |0\rangle\langle 0|$ . The solvable condition reads  $\text{Tr}_l[U(|0\rangle\langle 0| \otimes \rho)U^{\dagger}] = \text{Tr}[\rho] |0\rangle\langle 0|$  for any  $\rho$ , where the subscript  $l$  denotes the left site. In terms of Eq. (S33), the solvable condition can be rewritten as

$$\text{Tr}_l\{V[J_1, J_2, J_3][(v_- |0\rangle\langle 0| v_-^{\dagger}) \otimes (v_+ \rho v_+^{\dagger})]V^{\dagger}[J_1, J_2, J_3]\} = \text{Tr}[\rho] u_-^{\dagger} |0\rangle\langle 0| u_-. \quad (\text{S37})$$

We consider a *necessary condition* for this equation by taking  $\rho = I_2$ . To perform the trace operation, a trick is to rewrite the matrix  $V[J_1, J_2, J_3]$  as

$$V[J_1, J_2, J_3] = V[J'_1, J'_2, J'_3]V[\frac{\pi}{4}, \frac{\pi}{4}, \frac{\pi}{4}], \quad (\text{S38})$$

where  $V[\frac{\pi}{4}, \frac{\pi}{4}, \frac{\pi}{4}]$  is the SWAP gate exchanging the states of two qubits,  $J'_{\alpha} = J_{\alpha} - \frac{\pi}{4}$ ,  $-\frac{\pi}{4} \leq J'_{\alpha} < \frac{\pi}{4}$ . From now on, we will abbreviate the coefficients  $V_{\alpha}(J'_1, J'_2, J'_3)$  to  $V'_{\alpha}$ . Now, Eq. (S37) becomes

$$\text{Tr}_l\{V[J'_1, J'_2, J'_3][I_2 \otimes (v_- |0\rangle\langle 0| v_-^{\dagger})]V^{\dagger}[J'_1, J'_2, J'_3]\} = 2u_-^{\dagger} |0\rangle\langle 0| u_-. \quad (\text{S39})$$

We can calculate this equation by expanding the expression in the curly brackets on the Pauli basis of the left site, followed by the trace operation. It leaves

$$\sum_{\alpha=0}^3 |V'_{\alpha}|^2 (\sigma^{\alpha} v_- |0\rangle\langle 0| v_-^{\dagger} \sigma^{\alpha}) = u_-^{\dagger} |0\rangle\langle 0| u_-. \quad (\text{S40})$$



The left hand side is the summation of four rank-1 projectors with positive semi-definite coefficients, while on the right hand side there is one rank-1 projector. The equality holds only when the projector  $u_-^\dagger |0\rangle \langle 0| u_-$  is exactly the same as those projectors  $\sigma^\alpha v_- |0\rangle \langle 0| v_-^\dagger \sigma^\alpha$  with non-zero coefficients  $|V'_\alpha|^2$ .

We now show that it is impossible that three or all of  $V'_\alpha$  are non-zero. Consider the case that  $V'_\alpha$  and  $V'_\beta$  are non-zero, and thus  $\sigma^\alpha v_- |0\rangle$  and  $\sigma^\beta v_- |0\rangle$  are the same as  $u_-^\dagger |0\rangle$  up to a phase factor,  $\alpha \neq \beta$ . We can directly deduce that  $v_- |0\rangle$  is an eigenstate of  $\sigma^\alpha \sigma^\beta$ . If there is another non-zero coefficient  $V'_\gamma$ ,  $v_- |0\rangle$  should be an eigenstate of  $\sigma^\beta \sigma^\gamma$ , which is impossible because  $[\sigma^\alpha \sigma^\beta, \sigma^\beta \sigma^\gamma] \neq 0$ . Therefore, the three coefficients  $V'_{\alpha,\beta,\gamma}$  can not simultaneously be non-zero. Meanwhile, due to range of parameters  $-\frac{\pi}{4} \leq J'_\alpha < \frac{\pi}{4}$ ,  $V'_0$  can never be zero. Hence, we only need to consider the following two classes:

- (1)  $V'_0$  and one of  $V'_{\alpha \neq 0}$  are non-zero;
- (2) Only  $V'_0$  is non-zero.

We start from the first class and take  $\alpha = 3$  for instance. It follows that  $v_- |0\rangle$  and  $u_-^\dagger |0\rangle$  are eigenstates of  $\sigma^3$  with the same eigenvalue. We can therefore parameterize the single-site special unitaries as: (I)  $v_- = e^{-i\eta\sigma^3}$ ,  $u_- = e^{-i\epsilon\sigma^3}$ , or (II)  $v_- = i\sigma^1 e^{-i\eta\sigma^3}$ ,  $u_- = ie^{-i\epsilon\sigma^3} \sigma^1$ . As for the coefficients, we have

$$|V'_0|^2 + |V'_3|^2 = 1, V'_1 = V'_2 = 0, \quad (\text{S41})$$

of which the only solution is  $J'_1 = J'_2 = 0$ . It can be checked that this solution combined with (I) fulfill the original solvable condition Eq. (S37). This results in the set of unitary gates parameterized as Eq. (9) in the main text:

$$\begin{aligned} U &= e^{i\phi}(u_+ \otimes e^{-i\epsilon\sigma^3})V[0, 0, J'_3]V[\frac{\pi}{4}, \frac{\pi}{4}, \frac{\pi}{4}](e^{-i\eta\sigma^3} \otimes v_+) \\ &= e^{i\phi}(u_+ \otimes e^{-i\epsilon\sigma^3})V[\frac{\pi}{4}, \frac{\pi}{4}, J_3](e^{-i\eta\sigma^3} \otimes v_+). \end{aligned} \quad (\text{S42})$$

On the other hand, the single-site unitaries (II) can be included into Eq. (S42) through the following transformation:

$$\begin{aligned} U &= e^{i\phi}[u_+ \otimes (ie^{-i\epsilon\sigma^3} \sigma^1)]V[\frac{\pi}{4}, \frac{\pi}{4}, J_3][(i\sigma^1 e^{-i\eta\sigma^3}) \otimes v_+] \\ &= e^{i\phi}[(iu_+ \sigma^1) \otimes e^{-i\epsilon\sigma^3}]V[\frac{\pi}{4}, \frac{\pi}{4}, J_3][e^{-i\eta\sigma^3} \otimes (i\sigma^1 v_+)]. \end{aligned} \quad (\text{S43})$$

Other cases in the first class ( $\alpha = 1$  or  $2$ ) can be analyzed following a similar approach. It turns out that all the solutions are covered by Eq. (S42).

Next, we consider the second class, where  $V'_1 = V'_2 = V'_3 = 0$ . This condition leads to  $J'_\alpha = 0$ , and  $v_- u_- = e^{i\alpha}$ . The solutions read

$$U = e^{i\phi}(u_+ \otimes u_-)V[\frac{\pi}{4}, \frac{\pi}{4}, \frac{\pi}{4}](v_- \otimes v_+) = e^{i(\phi+\alpha)}(u_+ \otimes I_2)V[\frac{\pi}{4}, \frac{\pi}{4}, \frac{\pi}{4}](I_2 \otimes v_+), \quad (\text{S44})$$

which, again, are covered by Eq. (S42).

To conclude, we have exhausted the two-qubit gates fulfilling the solvable condition for  $\tilde{q} = 1$ . We obtain the solutions Eq. (S42) by rigorously classifying and discussing the consequences of a *necessary condition* Eq. (S39), while the solutions can be verified to fulfill the *sufficient condition*. We point out that all the gates given by Eq. (S39) are dual-unitary gates [8]. Remarkably, the solutions coincide with those two-qubit circuits characterized by chiral solitons [9], defined by the soliton condition:  $U^\dagger(\sigma^3 \otimes I)U = I \otimes \sigma^3$ .

### C. $q = 2, \tilde{q} = 2$

In this subsection we consider  $\tilde{q} = 2$  where  $\mathcal{H}_A = \mathcal{H}_{q=2}$ . Notice that solutions for  $\tilde{q} = 2$  must form a subset of solutions for  $\tilde{q} = 1$ . This observation provides us a convenient approach to parameterize the  $\tilde{q} = 2$  solutions, by applying the corresponding solvable condition on the  $\tilde{q} = 1$  solution to constrain the parameters  $J'_3, \epsilon$  and  $\eta$ . It follows that

$$\text{Tr}_l\{V[0, 0, J'_3][(v_+ \rho_r v_+^\dagger) \otimes (e^{-i\eta\sigma^3} \rho_l e^{i\eta\sigma^3})]V^\dagger[0, 0, J'_3]\} = \text{Tr}[\rho_r]e^{i\epsilon\sigma^3} \rho_l e^{-i\epsilon\sigma^3}, \quad (\text{S45})$$

which holds for arbitrary  $\rho_{l,r}$ . We take  $\rho_r = I_2$ , and expanding the matrix  $V$  on the Pauli basis, which gives:

$$\cos^2(J'_3)(e^{-i(\eta+\epsilon)\sigma^3} \rho_l e^{i(\eta+\epsilon)\sigma^3}) + \sin^2(J'_3)(\sigma^3 e^{-i(\eta+\epsilon)\sigma^3} \rho_l e^{i(\eta+\epsilon)\sigma^3} \sigma^3) = \rho_l. \quad (\text{S46})$$

The left hand side could be viewed as a quantum channel with two Kraus operators:  $K_0 = \cos(J'_3)e^{-i(\eta+\epsilon)\sigma^3}$ ,  $K_1 = \sin(J'_3)\sigma^3e^{-i(\eta+\epsilon)\sigma^3}$ . In this context, Eq. (S46) states that the quantum channel should be an identity operation, which requires that  $J'_3 = 0$ ,  $\eta + \epsilon = 0$ . The corresponding gates are

$$U = e^{i\phi}(u \otimes I_2)S, \quad (\text{S47})$$

where  $S = V[\frac{\pi}{4}, \frac{\pi}{4}, \frac{\pi}{4}]$  is the SWAP gate. It can be checked that all the gates in the form of Eq. (S47) fulfill the  $\tilde{q} = 2$  solvable condition.

- 
- [1] M. C. Bañuls, M. B. Hastings, F. Verstraete, and J. I. Cirac, “Matrix product states for dynamical simulation of infinite chains,” *Phys. Rev. Lett.* **102**, 240603 (2009).
  - [2] A. Müller-Hermes, J. I. Cirac, and M. C. Bañuls, “Tensor network techniques for the computation of dynamical observables in one-dimensional quantum spin systems,” *New J. Phys.* **14**, 075003 (2012).
  - [3] M. B. Hastings and R. Mahajan, “Connecting entanglement in time and space: Improving the folding algorithm,” *Phys. Rev. A* **91**, 032306 (2015).
  - [4] A. Leroise, M. Sonner, and D. A. Abanin, “Influence matrix approach to many-body floquet dynamics,” *Phys. Rev. X* **11**, 021040 (2021).
  - [5] F. Verstraete, J. J. Garcia-Ripoll, and J. I. Cirac, “Matrix product density operators: Simulation of finite-temperature and dissipative systems,” *Physical review letters* **93**, 207204 (2004).
  - [6] G. D. las Cuevas, N. Schuch, D. Pérez-García, and J. I. Cirac, “Purifications of multipartite states: limitations and constructive methods,” *New J. Phys.* **15**, 123021 (2013).
  - [7] B. Bertini, C. D. Fazio, J. P. Garrahan, and K. Klobas, “Exact quench dynamics of the floquet quantum east model at the deterministic point,” *arXiv:2310.06128* (2023).
  - [8] B. Bertini, P. Kos, and T. c. v. Prosen, “Exact correlation functions for dual-unitary lattice models in 1 + 1 dimensions,” *Phys. Rev. Lett.* **123**, 210601 (2019).
  - [9] B. Bertini, P. Kos, and T. Prosen, “Operator entanglement in local quantum circuits ii: Solitons in chains of qubits,” *SciPost Phys.* **8**, 068 (2020).
  - [10] N. Khaneja, R. Brockett, and S. J. Glaser, “Time optimal control in spin systems,” *Phys. Rev. A* **63**, 032308 (2001).
  - [11] B. Kraus and J. I. Cirac, “Optimal creation of entanglement using a two-qubit gate,” *Phys. Rev. A* **63**, 062309 (2001).
  - [12] J. Zhang, J. Vala, S. Sastry, and K. B. Whaley, “Geometric theory of nonlocal two-qubit operations,” *Phys. Rev. A* **67**, 042313 (2003).